Applied Catalysis B: Environmental 168 (2015) 540–549

Contents lists available at ScienceDirect

Applied Catalysis B: Environmental

journal homepage: www.elsevier.com/locate/apcatb

Ultra-low loading Ru/γ-Al_2O_3: A highly active and stable catalyst for low temperature solar thermal reforming of methane

David S.A. Simakov, Helen Y. Luo, Yuriy Román-Leshkov*

Department of Chemical Engineering, Massachusetts Institute of Technology, Cambridge, MA 02139, USA

ARTICLE INFO

Article history:
Received 23 October 2014
Received in revised form
29 December 2014
Accepted 9 January 2015
Available online 13 January 2015

Keywords:
Methane reforming
Catalyst
Ruthenium
Solar reforming
Ultra-low loading

ABSTRACT

Converting solar radiation into chemical energy is an attractive method to increase the energy content of methane by driving endothermic upgrading processes, such as methane steam reforming. Although such solar thermochemical conversions would increase natural gas product yields and reduce greenhouse gas emissions, current costs of solar facilities are prohibitively high. Parabolic troughs, which are a mature and relatively inexpensive form of solar concentrator, are limited to temperatures of ca. 400–600 °C. In this regime, commercial methane steam reforming Ni-based catalysts have low activity and rapidly deactivate due to oxidation and coking. Catalysts based on platinum group metals are much more active and stable but their high cost limits their use. Here, we investigate Ru-based catalysts with ultra-low metal loadings for low-temperature methane steam reforming. We show that a Ru/γ-Al_2O_3 (0.15 wt% loading) catalyst outperforms the commercial (12 wt% Ni) catalyst by two orders of magnitude in terms of methane conversion normalized by metal loading. Systematic evaluation of catalytic performance over a range of Ru loadings and operating conditions shows a pronounced optimum in catalytic activity versus metal loading. Characterization studies reveal a strong correlation between the catalytic activity and the Ru nanoparticle size distribution. The catalyst features excellent stability at industrially relevant conditions and low steam-to-carbon ratios, making it an attractive option for low-temperature solar reforming of methane.

© 2015 Elsevier B.V. All rights reserved.

1. Introduction

In solar thermochemical processes [1], concentrated solar radiation is used to drive highly endothermic reactions, such as methane steam reforming (MSR, Eq. (1)). MSR is the most widely used method to produce synthesis gas (syngas) and hydrogen (H_2) on a commercial scale. MSR is accompanied by the water gas shift (WGS, Eq. (2)) reaction that increases the fraction of H_2 in the outlet stream. In industrial reformers (operated at ca. 850–950 °C), the necessary heat to drive the endothermic MSR process is generated by combusting a fraction of the natural gas fed (ca. 30%). This fraction can be saved by the use of solar energy as a source of heat, increasing the overall yield of the process [2–4]. The resulting "solar" syngas can be used as a chemical feedstock or as a fuel for electricity generation in gas turbines [3,5].

$$CH_4 + H_2O \rightleftarrows CO + 3H_2 \qquad \Delta H_{298}^{\circ} = 206\,\text{kJ/mol} \qquad (1)$$

$$CO + H_2O \rightleftarrows CO_2 + H_2 \qquad \Delta H_{298}^{\circ} = -41\,\text{kJ/mol} \qquad (2)$$

Solar dishes and central receivers are the only solar concentrators capable of achieving the high temperatures required for complete MSR conversions. Unfortunately, their high capital costs hinder the economic viability of the process [1]. In contrast, parabolic trough solar concentrators (commonly used in conventional concentrated solar power plants) are relatively inexpensive but restricted to temperatures below 600 °C [1]. Although at these temperatures the CH_4 conversion is below 50%, complete conversions are not always necessary, especially for applications such as electricity generation via gas turbines. Fig. 1a shows the calculated equilibrium CH_4 conversions of the combined MSR-WGS process [6]. The corresponding values of the fuel upgrade factor, defined in Eq. (3), are depicted in Fig. 1b.

$$\text{fuel upgrade\%} = 100\left[\frac{(1-f_1)\times LHV_{CH_4} + f_2 \times LHV_{CO} + (4f_1 - f_2)\times LHV_{H_2}}{LHV_{CH_4}} - 1\right] \qquad (3)$$

$$f_1 = \frac{F_{CH_4,f} - F_{CH_4,eq}}{F_{CH_4,f}}; \qquad f_2 = \frac{F_{CH_4,f} - F_{CH_4,eq} - F_{CO_2,eq}}{F_{CH_4,f}}$$

In Eq. (3) f_1 is total CH_4 conversion and f_2 is conversion of CH_4 to CO (F is molar flow rate and subscripts f and eq refer to feed and equilibrium outlet flows, respectively). The low heating values (LHVs) of CH_4, CO and H_2 are 802.3, 241.8 and 283.2 kJ/mol, respectively. Based on these values, the maximum fuel upgrade at

* Corresponding author. Tel.: +1 617 258 0431; fax: +1 617 324 0060.
E-mail address: yroman@mit.edu (Y. Román-Leshkov).

http://dx.doi.org/10.1016/j.apcatb.2015.01.011
0926-3373/© 2015 Elsevier B.V. All rights reserved.

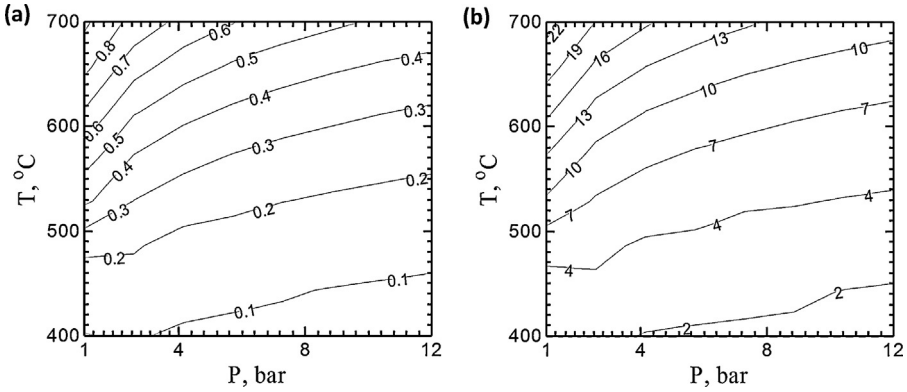

Fig. 1. Equilibrium CH_4 conversion (a) [6] and corresponding fuel upgrade percent (b), Eq. (3), of the combined MSR-WGS process as a function of pressure and temperature.

full conversion is 26.5%. Importantly, we can achieve significant fuel upgrade factors of 10–15% by reforming at $T = 550–600\,^{\circ}C$ and $P < 5$ bar (Fig. 1b), providing a significant increase in feed utilization, and ultimately in electrical power output. However, a difficult challenge exists in designing affordable and stable catalysts that can effectively operate in the low temperature regime.

In commercial installations, MSR is catalyzed by nickel (Ni) supported on aluminum oxide (α-Al_2O_3) with metal loadings ranging from 10–18 wt%. Although Ni is inexpensive and features reasonable catalytic activity, it rapidly deactivates by coke deposition especially at steam-to-carbon ratios below 3 [7–9]. On the other hand, low steam-to-carbon ratios are preferable for solar thermal reforming facilities that require high capital cost investment, because handling large amounts of excess steam will further increase the cost. Moreover, Ni-based catalysts have insufficient activity and deactivate rapidly via oxidation at low temperatures [10]. In contrast, platinum group metals (PGMs) are much more active and have been identified as excellent MSR catalysts [11–17]. Supported PGMs exhibit better stability to deactivation by sintering, oxidation, and coking than Ni-based catalysts. Progress toward the use of PGMs for low-temperature MSR was outlined in a recent review [10]. Although there is still disagreement on which PGM has the highest activity [11,18], Ru is preferred due to its relative lower price compared to other PGMs. The major challenge in implementing Ru for MSR is the cost associated with current catalyst formulations, which feature prohibitively high metal loadings (typically ranging from 1–5 wt%). While the penalty associated with the use of a more expensive catalyst can be compensated to some extent by superior catalytic performance, metal loadings have to be reduced drastically for these catalysts to be of commercial interest.

Herein, we addressed this challenge by determining the lower limit of the active phase loading of the Ru/γ-Al_2O_3 catalyst that can provide high activity and stability in low temperature MSR at the same time. The sonication-assisted preparation route was implemented in order to maximize the active phase dispersion. We demonstrate that Ru/γ-Al_2O_3 catalysts prepared with ultra-low metal loadings are highly active and stable for MSR at low temperatures. The 0.15 wt% Ru/Al_2O_3 catalyst outperforms the commercial (12 wt% Ni/α-Al_2O_3) catalyst by two orders of magnitude in terms of methane conversion rate per active metal loading, while also providing excellent stability at low steam-to-carbon ratios and elevated space velocities. Catalyst performance was tested under varying operating conditions and over a wide range of metal loadings (0.07–3 wt%), including ultra-low loading formulations as well as loadings typically applied in commercial applications (1 and 3 wt%) for comparison.

Currently, there are no studies that provide quantitative insights with regards to the lower limit of the active phase loading for PGM-based MSR catalysts. The data on the effects of the ultra-low loading formulations on catalytic activity and stability are lacking. Systematic studies of catalytic performance over a wide range of operating conditions are also lacking, in particular of industrially-relevant conditions such as elevated space velocities. Our findings show a strong correlation between the turn over frequency (TOF) and the active phase loading, with a pronounced maximum for 0.15 wt% Ru loading. The characterization study points at the strong Ru nanoparticle size-catalytic activity relationship. The low PGM loading formulation coupled with high activity and exceptional stability makes this catalyst of high interest for potential applications of distributed power and fuels generation via low-temperature solar thermal reforming using parabolic troughs. The applicability is yet to be determined, however, in a real solar reforming experiment that will impose additional requirements, e.g. stability with respect to fluctuations in heat supply.

2. Experimental

2.1. Catalyst preparation

Ru/γ-Al_2O_3 catalysts with different Ru loadings of 0.07, 0.15, 0.30, 1 and 3 wt% were synthesized by sonication-assisted wet impregnation using ruthenium (III) chloride hydrate ($RuCl_3 \times H_2O$, 38% Ru, Alfa Aesar) as a precursor, high surface area aluminum oxide (γ-Al_2O_3, 220 m^2/g, 1/8" pellets, Alfa Aesar) as a support, and acetone (99.5% purity, Alfa Aesar) as an impregnation medium. Prior to impregnation, the support pellets were sieved to 250–425 μm. Appropriate amounts of $RuCl_3 \times H_2O$ were dissolved in acetone, the support particles were subsequently added and the resulting slurries were placed in an ultrasonic bath (Branson 5510) in glass vials for 30 min. After sonication, acetone was evaporated from the slurries at 55 °C. A commercial Ni/α-Al_2O_3 catalyst (12 wt% Ni, BASF, supplied by Research Catalysts, Inc. USA) sieved to 250–425 μm pellets was used as a reference.

2.2. Catalytic activity evaluation

Catalyst precursors ($RuCl_3$ dispersed on a high surface area γ-Al_2O_3, prepared as described in the previous section) were loaded into a stainless steel ″T″ union (1/4″, Swagelok) connected to a 1/4″ stainless steel tubes (Swagelok), between two pieces of quartz wool. The volume of the catalytic bed was ca. 0.2 mL. Intraparticle and interparticle transport limitations were ruled out using the criteria for heat and mas transfer resistance described in Eq. (4) [19], using the steam reforming kinetic parameters of apparent activation energy $E_{MSR} = 91$ kJ/mol and pre-exponential factor of $A_{MSR} = 4.7 \times 10^4$ s^{-1} kPa^{-1} previously obtained by Wei and Iglesia for Ru/Al_2O_3 catalysts [20]. All calculations showed that under

the reaction conditions investigated, no mass or heat transfer limitations are present.

$$\phi^2 \equiv \frac{k_{MSR} d_p^2}{4D} << 1 \quad \text{(T h iele Modulus)}$$

$$\frac{|\Delta H_{MSR}| \epsilon \rho_g k_{MSR} d_p^2}{4 k_g T} << \frac{0.75 T R_g}{E_{MSR}} \quad \text{(isothermal catalytic pellet criterion)}$$

$$\frac{k_{MSR} d_p}{2 y_{CH_4,f} \rho_g k_c} << 0.15 \quad \text{(interphase mass transfer criterion)} \qquad (4)$$

$$\frac{|\Delta H_{MSR}| \epsilon \rho_g k_{MSR} d_p}{2 h_{gs} T} << \frac{0.15 T R_g}{E_{MSR}} \quad \text{(interphase heat transfer criterion)}$$

$$k_{MSR} = A_{MSR} \exp\left(-\frac{E_{MSR}}{R_g T}\right)$$

Catalytic activity evaluation was carried out using a continuous flow system controlled and monitored by a computer with a continuous data recording (LabVIEW, National Instruments Corporation), Fig. 2. The reactor was heated in an electric furnace (model 3210, Applied Test Systems, Inc.) equipped with a temperature controller (model 68,900-10, Digi-Sense). A K-type thermocouple (OMEGA Engineering, Inc.) was placed inside the reactor tube in a contact with the catalyst bed. Analog-to-digital/digital-to-analog converters (model NI USB-9263, NI USB-9215, NI USB-9211, NI cDAQ-9184, National Instruments Corporation) were used to control gas flow via mass flow controllers (model 5850TR, Brooks Instrument) and water supply via a syringe pump (model NE-8000, New Era Pump Systems Inc. USA), and to monitor flow rates and temperature continuously. Pressure was regulated using a back pressure regulator (model 44-2363-24, TESCOM Corporation, USA). Concentrations of CH_4, CO and CO_2 were measured using an infrared analyzer (model IR-208, Infrared Industries, Inc. USA) on a dry basis, after removal of water condensate by a water trap (model NAFM4000-N02, SMC Corporation of America) and residual humidity by a column packed with orange silica gel pellets (2–5 mm, Sigma–Aldrich), Fig. 2.

For each Ru loading (and for the Ni-based commercial catalyst), the catalyst was first reduced in situ in flowing H_2 (200 mL/min) by ramping to 600 °C with a heating rate of 10 °/min with a subsequent isothermal step at 600 °C for 1 h. The feed stream was then switched to a mixture of CH_4 and H_2O. Each catalyst was then tested over a range of temperatures (400–600 °C) and at space velocity of GHSV = 750 mL/(g h) to test for approach to equilibrium (at such a low space velocity equilibrium is expected to be attained). Gas hourly space velocity (GHSV) is defined as the ratio of the volumetric CH_4 feed rate (calculated at standard conditions) and the catalyst bed weight:

$$\text{GHSV} = \frac{Q^{\text{STP}}_{CH_4,f}}{W_c} \qquad (5)$$

For each sample, catalytic performance was subsequently evaluated for four sets of operating conditions, varying pressure (P), temperature (T) and steam-to-carbon ratio (S/C). The following sequence was used for all samples: (i) P = 1 bar, T = 600 °C, S/C = 3; (ii) P = 5 bar, T = 600 °C, S/C = 3; (iii) P = 1 bar, T = 500 °C, S/C = 3 and (iv) P = 5 bar, T = 600 °C, S/C = 1. Different sets of operating conditions were selected in order to evaluate catalyst performance in different regimes. It is well known that optimal conditions for MSR are low P, high T and high S/C (set (i)) and elevated P results in significantly lower conversions (set (ii)), while deactivation is likely to occur at low T with oxidant in excess (set (iii)) and coking is susceptible for low S/C (set (iv)). For each set, catalytic activity was evaluated over a range of space velocities of GHSV = 750 – 30,000 mL/(g h), in order to evaluate kinetic limits. For each space velocity tested, it was verified that steady state conversion and selectivity (to CO) were attained which required ca. 30 min for GHSV < 10,000 mL/(g h) and less than 15 min for higher space velocities. Accordingly, each value of GHSV was tested for 1 h for GHSV < 10,000 mL/(g h) and for 30 min for higher values. Finally, a stability test was performed for 48 h. For each catalyst tested, the total time on stream was 160 h and *these spent samples were used for characterization*. For selected catalyst formulations, longer stability tests were performed (> 100 h). After the test, the reactor was flushed with He (50 mL/min) for 30 min and cooled down to room temperature. Spent catalysts were stored in sealed vials prior to characterization.

Carbon balance (CB), methane conversion (f) and selectivity to CO (Y) were evaluated based on volumetric fractions measured in the outlet feed *on a dry basis*:

$$\text{CB} = y_{CH_4} + 4y_{CO} + 5y_{CO_2} \qquad (6)$$

$$f = \frac{y_{CO} + y_{CO_2}}{y_{CH_4} + y_{CO} + y_{CO_2}} \qquad (7)$$

$$Y = \frac{y_{CO}}{y_{CO} + y_{CO_2}} \qquad (8)$$

Coefficients of 4 and 5 in Eq. (6) account for the increase in a number of moles as a result of MSR and combined MSR–WGS processes (Eqs. (1) and (2)), i.e. Eq. (6) counts the measured volumetric fractions of CH_4, CO, CO_2 and the volumetric fraction of H2 (3 and 4 moles of H2 are generated per each mole of CO and CO2 produced, respectively); the total should be unity if there is no carbon deposition. Carbon balance was continuously monitored and recorded and it was verified that deviations from 100% do not exceed ± 5%. Methane conversion rates per catalyst bed weight (W_c) and per weight of the active phase were calculated by Eqs. (9) and (10), respectively (L_{Me} is percentage metal loading):

$$r = \frac{F_{CH_4,f} f}{W_c} \qquad (9)$$

$$R = \frac{r}{(L_{Me}/100)} \qquad (10)$$

TOF was calculated by the following equation:

$$\text{TOF} = \frac{M_{W,Me}}{D} R_{max} \qquad (11)$$

In Eq. (11), $M_{W,Me}$ and D stand for metallic phase molecular weight and dispersion, respectively. R_{max} denotes the upper limiting value of the CH_4 conversion rate (Eq. (10)) attained at high space velocities, i.e. far from equilibrium, when further increase in space velocity does not result in an increase in CH_4 conversion rate (Fig. 4 in Section 3.1).

2.3. Characterization of spent catalysts

Phase analysis of the spent catalysts was determined from powder X-ray diffraction (PXRD) patterns collected using a Bruker D8 diffractometer using Cu Kα radiation (40 kV, 40 mA). Thermogravimetric analysis (TGA) coupled with mass spectroscopy (MS) was performed on spent catalysts to determine the extent of coking. TGA was performed with a TA instruments TGA Q500 under air flow of 50 ml/min at a ramp rate of 5 °C/min up to 900 °C. The CO_2 content of the gas stream was tracked with a Hiden HPR-20 WIC TMS transient MS equipped with an Edwards turbo pump and controller. Transmission electron microscopy (TEM) images were obtained to determine particle size distributions for spent catalysts. Catalyst samples were first dispersed in acetone before depositing on 300 mesh copper grids. Images were taken using a JEOL 2010 F with a Schottky field emission gun operating at 200 kV, equipped with a CCD camera. For each sample, 150–200 individual particles were measured with image processing software (ImageJ) to determine the particles size distribution. Active phase dispersion was calculated using the following equation that accounts

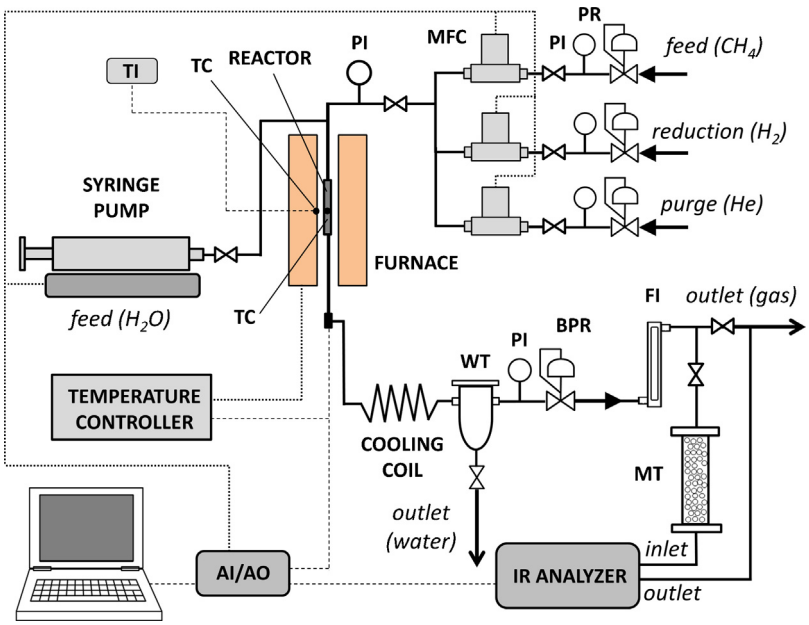

Fig. 2. Experimental system for catalytic activity evaluation: AI/AO – analog input/output module (analog-to-digital/digital-to-analog converter), BPR – backpressure regulator, FI – flow indicator (rotameter), IR – infrared, MFC – mass flow controller, MT – moisture trap (silica gel), PI – pressure indicator, PR – pressure reducer, TC – thermocouple, TI – temperature indicator, WT – water trap.

for polydispersity:

$$D(\mathrm{TEM}) = 100\frac{N_S}{N_V} = \frac{100}{V_t}\sum_i^{d_{p,\max}} \frac{\pi d_{p,i}^2}{A_{Ru}} \frac{6}{N_A \rho_{Me} \pi d_{p,i}^3} \frac{\pi d_{p,i}^3}{6} f_i V_t$$

$$= \sum_i^{d_{p,\max}} \frac{\pi d_{p,i}^3}{6} f_i \qquad (12)$$

The active phase dispersion was also calculated from CO chemisorption isotherms measured on a Quantachrome Autosorb iQ apparatus. Samples were first reduced in flowing H_2 (2 h, 350 °C, 20 °C/min ramp), evacuated for 2 h at 350 °C to remove chemisorbed hydrogen and then cooled to the adsorption temperature under vacuum. CO chemisorption was performed at 35 °C, and analysis was performed by collecting an adsorption isotherm to determine total uptake, evacuating the sample to remove physisorbed H_2 (1 h), and collecting a second isotherm.

3. Results and discussion

3.1. Catalyst performance

Fig. 3 shows CH_4 conversion (f, Eq. (7)) and selectivity to CO (Y, Eq. (8)) measured for 3 wt% (Fig. 1(a)) and 0.15 wt% (Fig. 1(b)) Ru/γ-Al_2O_3 catalysts over the 400–600 °C temperature range at GHSV = 750 mL/(g h) and for two different S/C ratios. It can be seen that both f and Y attain their equilibrium values. This reactivity screening test was performed for each sample and our results confirmed that equilibrium values were indeed attained for all catalysts at GHSV = 750 mL/(g h).

As expected, increasing the space velocity results in a decline in CH_4 conversion, Fig. 4(a). As the reaction departs from the equilibrium, the rate of CH_4 conversion (Eq. (9)) increases, approaching the initial rate value, Fig. 4(b) (0.026 mol/(kg s) for this particular case). For all samples, initial rates were measured in the same manner, i.e. by increasing the space velocity until the maximum value of the CH_4 conversion rate is attained. These rates were then normalized to the metal loading in order to calculate the turnover frequency (Eq. (11)). We note that there is a notable decrease in selectivity to CO that occurs with increasing space velocity (Fig. 4(a)).

Fig. 5 compares the CH_4 conversion rate of the ultra-low loading Ru/γ-Al_2O_3 catalysts (0.15 and 0.3 wt% of Ru) and of the commercial 12 wt% Ni/α-Al_2O_3 catalyst. The comparison was performed under three different sets of operating parameters, including conditions that can lead to catalyst oxidation and coking (see Section 2.2 for details) and over a wide range of space velocities. Fig. 5(a) shows rates per total weight of catalyst (metallic phase and support), which are significantly higher for Ru-based catalysts despite the two orders of magnitude difference in the active phase loading. This dissimilarity is even more pronounced when rates are calculated per amount of the metallic phase, as it is shown in Fig. 5(b–d). The operating conditions tested included S/C = 1 that promotes carbon formation and T = 500 °C that favors oxidative deactivation. For all conditions, the ultra-low loading Ru catalysts were ca. two orders of magnitude more active in CH_4 conversion than the commercial catalyst with 12 wt% Ni loading in the full range of space velocities. Specifically, the 0.15 wt% Ru and the 12 wt% Ni catalysts featured methane conversion rates of ca. 50–100 mol/(kg(Ru) s) and ca. 0.5–1 mol/(kg(Ni) s), respectively, at a space velocity of 30,000 mL/(g h). Note that this space velocity corresponds to a contact time of 60 ms (industrial reformers are typically operated at contact times of few seconds).

CO selectivity for different Ru loading is shown in Fig. 6. For all loadings, except for 0.07 wt% Ru, selectivity was close to that expected at equilibrium. Overall, it was observed that CO selectivity decreased with increasing space velocity by ca. 20–30% over the 1000–30,000 mL/(g h) GHSV range. For the 0.07 wt% Ru sample selectivity to CO was significantly lower than that predicted by equilibrium. Interestingly, the 0.07 wt% Ru catalyst was also much less active than the 0.015 wt% Ru formulation (Section 3.3).

3.2. Spent catalyst characterization

Fig. 7 shows XRD patterns of spent Ru/γ-Al_2O_3 catalysts (after total 160 h on stream, see Section 2.2). The diffractograms show that the support phase, γ-Al_2O_3, maintains its structure, which

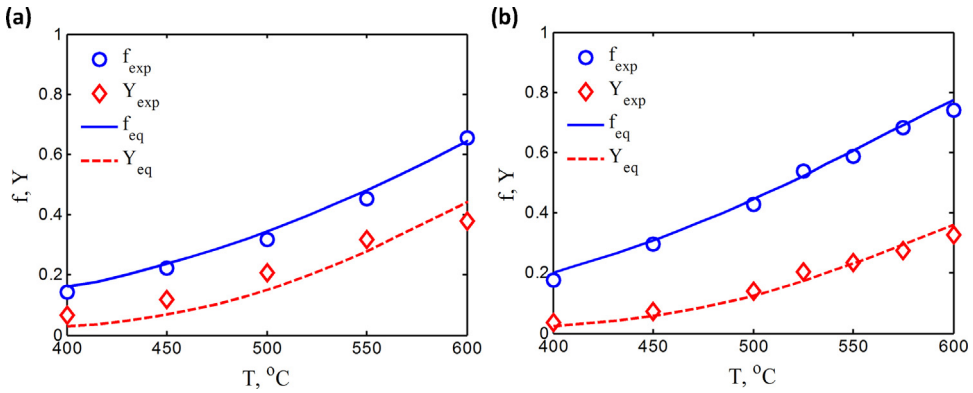

Fig. 3. Approach to equilibrium: CH_4 conversion (f) and selectivity to CO (Y) measured at GHSV = 750 mL/(g h) are shown as a function of temperature for 3 wt% Ru/γ-Al_2O_3 at a $S/C = 2$, $P = 1$ bar (a) and 0.15 wt% Ru/γ-Al_2O_3 at $S/C = 3$, P = 1 bar (b). Symbols show experimental measurements and lines represent equilibrium values.

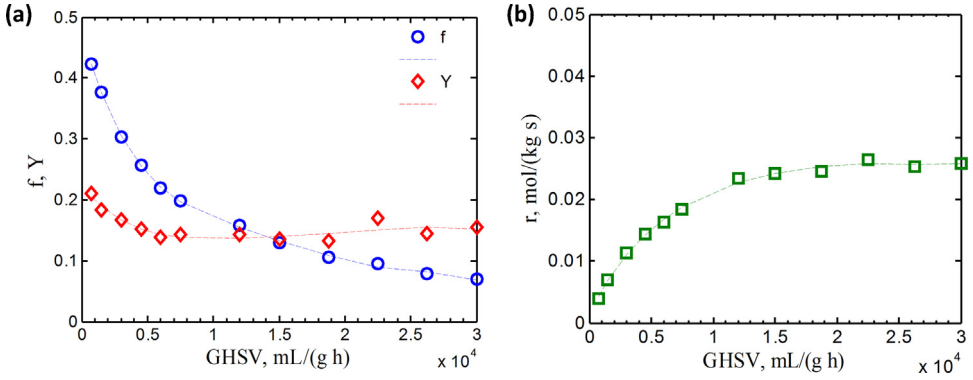

Fig. 4. Approach to kinetic limit: CH_4 conversion (f), selectivity to CO (Y) (a) and CH_4 conversion rate (b) are shown as a function of space velocity (GHSV) for 0.3 wt% Ru/γ-Al_2O_3 evaluated at $P = 1$ bar, $S/C = 3$ and $T = 500\,^{\circ}C$. Equilibrium CH_4 conversion is 0.45 under these conditions.

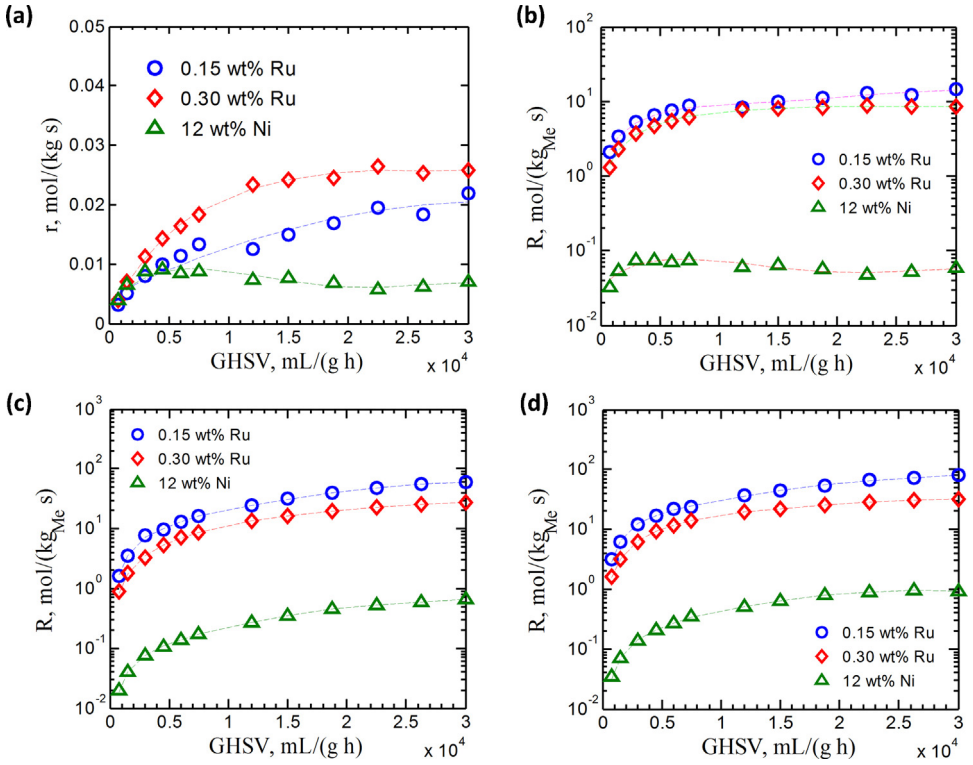

Fig. 5. Rate of CH_4 conversion per total supported catalyst weight (a) and per active (metal) phase weight (b–d) as a function of space velocity (GHSV) measured under different operating conditions: $P = 1$ bar, $S/C = 3$, $T = 500\,^{\circ}C$ (a, b); $P = 5$ bar, $S/C = 1$, $T = 600\,^{\circ}C$ (c) and $P = 5$ bar, $S/C = 3$, $T = 600\,^{\circ}C$ (d). Catalytic activity of the ultra-low loading Ru/γ-Al_2O_3 catalysts (0.15 wt% and 0.30 wt% Ru) is compared to the activity of the commercial 12 wt% Ni/α-Al_2O_3 catalyst.

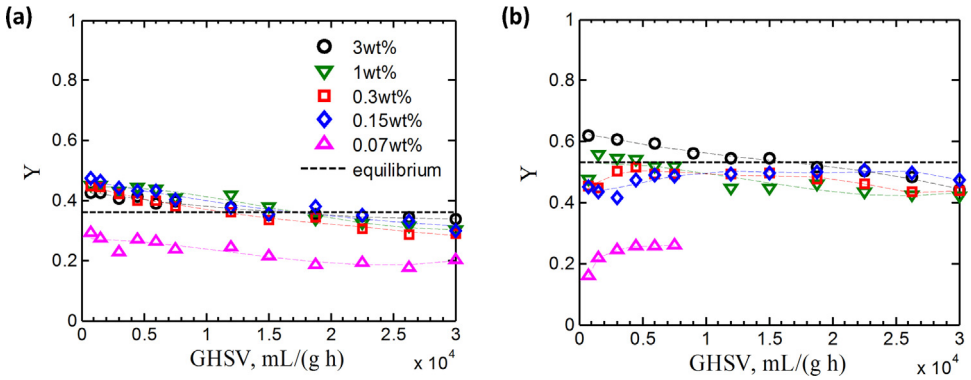

Fig. 6. Selectivity to CO (Y) as a function of space velocity (GHSV) for the range of Ru loading (0.07–3 wt%) measured under two sets of operating conditions: P = 1 bar, S/C = 3, T = 600 °C (a) and P = 5 bar, S/C = 1, T = 600 °C (b). Equilibrium values are shown for comparison (dashed line).

is expected because of the low reaction temperature. Ruthenium peaks were difficult to identify due to low loadings and peak broadening. Broad peaks were detected (shown by stars in Fig. 7(b)) that correspond to a metallic Ru phase, as seen for the commercial Ru/γ-Al_2O_3 sample (Fig. 7(a)). The very significant peak broadening is a result of the small nanocrystallite size as also evidenced from TEM analysis (vide infra). The combined effect of peak broadening and overlapping in the diffractograms prevented us from determining average crystallite sized based on the Scherrer equation.

Thermogravimetric analysis (TGA) of spent catalysts is shown in Fig. 8(a). Except for the initial weight loss due to physically adsorbed water, all catalysts had a similar weight loss ranging from 2.4 to 3.1% (after 100 °C). These values are slightly lower than the corresponding weight loss measured for the unused commercial γ-Al_2O_3 support (5.4%). Due to very low Ru loadings, the weight gain from Ru oxidation is rather insignificant (maximum 1% weight gain is expected for 3 wt% Ru catalyst as Ru is oxidized to RuO_2 and much less for lower loadings). Therefore, the difference in weight loss between the spent catalysts and the support cannot be attributed to Ru oxidation during the TGA experiment. Consequently, the difference in weight loss between the spent catalysts and the fresh γ-Al_2O_3 support (2.4–3.1% vs. 5.4%) is rather associated with the support dehydration during the reforming experiment due to elevated temperature. As it can be clearly seen from Fig. 8(a), a significant weight loss occurs for the γ-Al_2O_3 support as it is heated to 600 °C.

The absence of a significant amount of coke in the spent Ru catalysts is evident from the TGA-MS analysis (Fig. 8(b,c)) and from visual examination (Fig. 8(d,e)) using the commercial Ni/α-Al_2O_3 catalyst as a reference. The presence of the significant extent of coking for the Ni/α-Al_2O_3 catalyst can be clearly seen from the TGA-MS analysis (Fig. 8(b)) that shows pronounced peaks of CO_2 released at 400–650 °C (the increase in weight is due to Ni oxidation). No such peak was detected for the 0.15wt% Ru/γ-Al_2O_3 spent catalyst (Fig. 8(c)). Therefore, the small weight loss measured for Ru-based spent catalysts should be attributed to the dehydration of the γ-Al_2O_3 during the TGA experiment rather than removal of coke.

TEM micrographs of the spent catalysts are shown in Fig. 9. In all Ru-based samples, Ru nanocrystallites in two size domains were found: one with typical sizes of ca. 2–3 nm (Fig. 9(a)) and another with sizes of ca. 4–10 nm (Fig. 9(b)). As expected, much larger particles were found in the spent Ni/α-Al_2O_3 catalyst (Fig. 9(c)). Particle size distributions calculated from TEM images (TEM PSD) are shown in Fig. 9(d). Samples with 0.3, 1 and 3 wt% Ru have a bimodal distribution, while samples with 0.07 and 0.15 wt% Ru have a unimodal distribution centering around 2–3 nm even after 160 h on stream. Dispersions calculated from TEM PSD (Eq. (12)) are shown in Fig. 9(e), as a function of Ru loading. Note that the apparent decrease in dispersion for 0.07 wt% Ru could be the result of formation of sub-nanometer Ru clusters, which are undetectable by TEM. Formation of such clusters is expected at a significant extent for such low loadings of metallic phase. Active phase dispersion was also evaluated using CO chemisorption.

Table 1 compares values of dispersion calculated by both methods, along with average particle size and dispersity (determined by TEM PSD). The dispersion values obtained by chemisorption are consistently lower than those calculated with TEM, but the general trend is very similar across samples. Note that the difference in dispersion between 0.07 and 0.15 wt% of Ru is much less pronounced

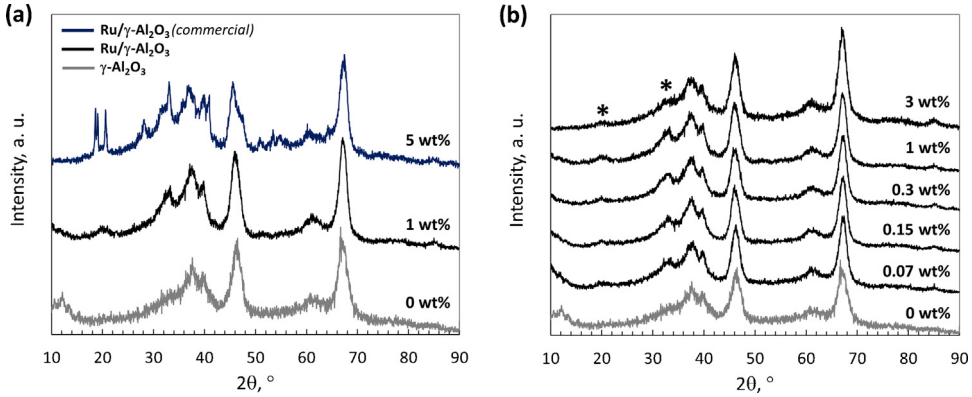

Fig. 7. XRD of spent (160 h on stream) Ru/γ-Al_2O_3 catalysts with different loadings. Commercial γ-Al_2O_3 support used for catalyst synthesis (0 wt% in (a)) and commercial 5 wt% Ru/γ-Al_2O_3 catalyst (fresh reduced, 5 wt% in (a)) are shown for comparison.

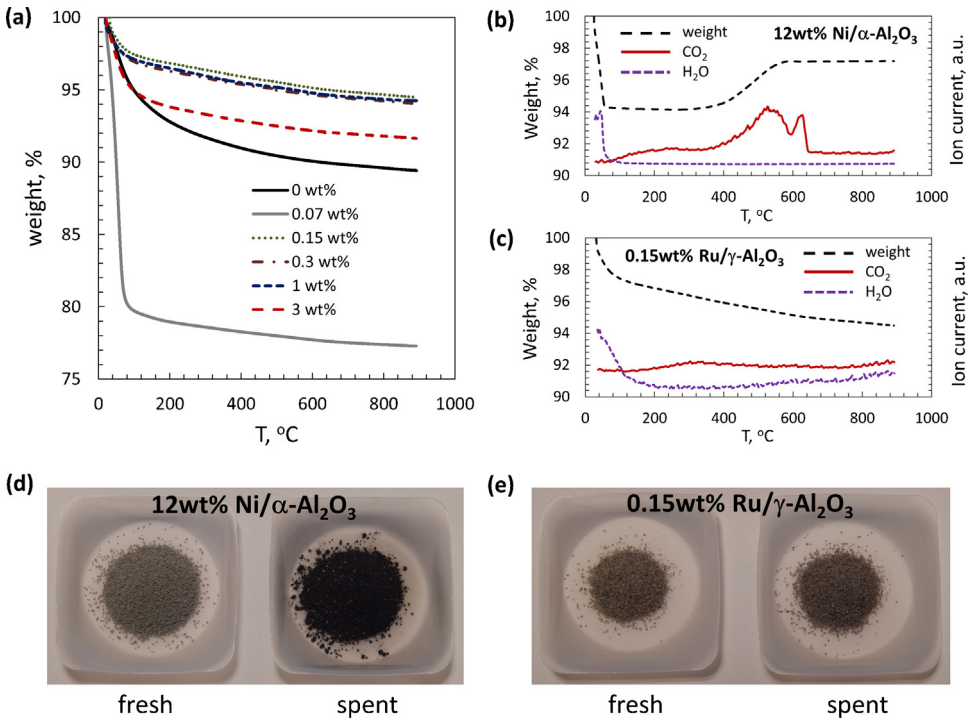

Fig. 8. TGA of spent (160 h on stream) Ru/γ-Al_2O_3 catalysts with different Ru loadings (a) and TGA-MS (b, c) of spent commercial 12 wt% Ni/α-Al_2O_3 (b) and 0.15 wt% Ru/γ-Al_2O_3 (c) catalysts (160 h on stream). TGA of γ-Al_2O_3 support is shown for comparison in (a) as 0 wt%. Photographs of fresh (reduced) and spent catalysts are also shown (d, e).

when measured by chemisorption, as compared to TEM. Since the chemisorption method accounts for all surface sites, including sub-nanometer clusters, this observation can be interpreted as additional, indirect evidence for the presence of sub-nanometer Ru clusters.

3.3. Catalytic activity

Fig. 10 shows measured turnover frequency (TOF, Eq. (11)) plotted as a function of Ru loading. TOF values were calculated using dispersion measured by chemisorption, as well as dispersion cal-

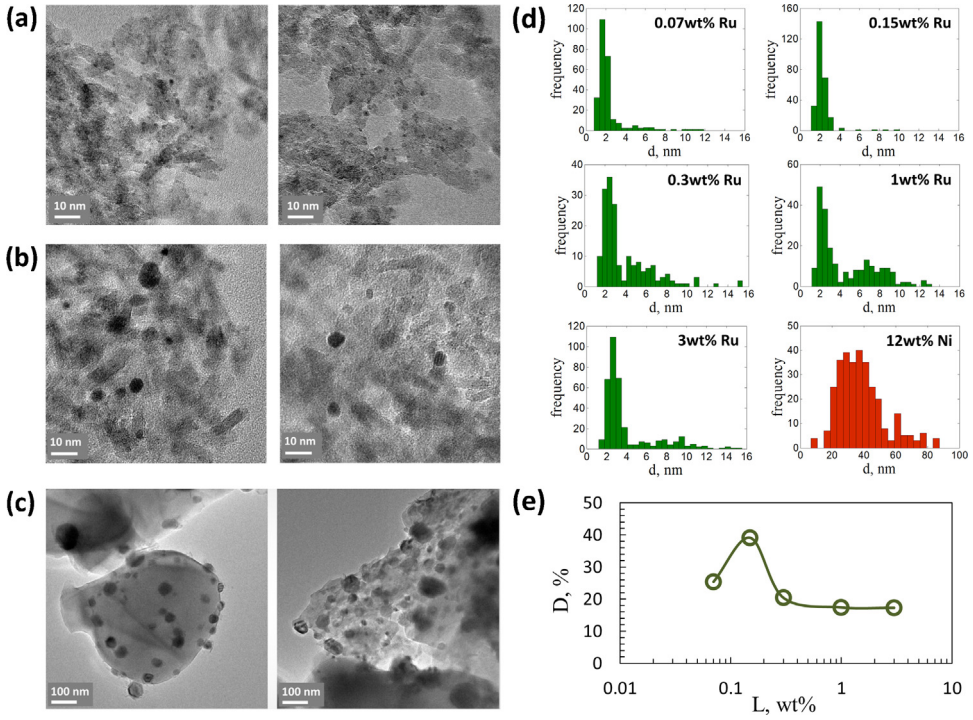

Fig. 9. TEM micrographs (a–c) and particle size distributions (PSDs) calculated from TEM (d) of spent catalysts (160 h on stream). Two types of Ru nanoparticles found in spent catalysts (a, b) and Ni nanocrystallites (c) are shown in representative TEM micrographs. Active phase dispersion calculated from TEM PSDs (d) using Eq. (7) is shown in (e) as a function of Ru loading.

Table 1
Active phase nanoparticle diameter (d_p) and dispersion (D) calculated from TEM PSDs (Fig. 4(d)) and chemisorption (CS). Dispersity is also shown as standard deviation of TEM PSD (σ).

L_{Me}, (wt%)	d_p (TEM), (nm)	σ (TEM), (nm)	D (TEM), (%)	D (CS), (%)	d_p (CS), (nm)
Ru/γ-Al_2O_3					
0.07	2.3	1.6	25.4	22.1	6.0
0.15	2.2	0.8	39.1	27.0	4.9
0.3	3.9	2.6	20.4	17.9	7.4
1	4.8	3.5	17.4	14.1	9.3
3	4.0	2.7	17.3	21.8	6.1
Ni/α-Al_2O_3					
12	38.5	14.8	2.1	5.9	17.1

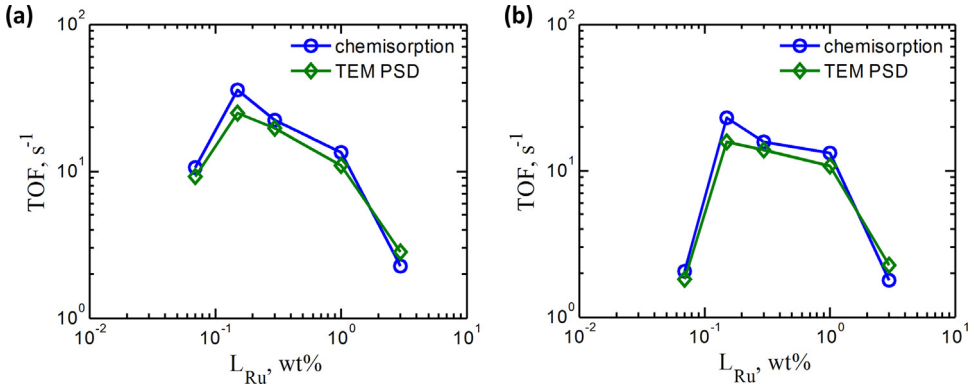

Fig. 10. Turnover frequency (TOF) values based on metal phase dispersion calculated from chemisorption and from TEM particle size distribution (Eq. (12), denoted as TEM PSD) for Ru/γ-Al_2O_3 catalysts as a function of the active phase (Ru) loading. TOF values measured under two sets of operating conditions are shown: P = 1 bar, S/C = 3, T = 600 °C (a) and P = 5 bar, S/C = 1, T = 600 °C (b). For comparison, TOF = 0.6 (1.7) s^{-1} and 0.7 (1.9) s^{-1} were measured for 12 wt% Ni/α-Al_2O_3 commercial catalyst under identical conditions, (a) and (b), respectively, based on dispersion calculated either with two H_2 chemisorption or from the particle size distribution (PSD) obtained by TEM (shown in brackets).

culated by Eq. (12) from particle size distributions obtained by TEM (denoted as TEM PSD in Fig. 10). For two different sets of operating conditions, a pronounced optimum in TOF was observed, with a highest TOF of ca. 40 s^{-1} obtained for the 0.15 wt% Ru/γ-Al_2O_3 catalyst at 600 °C, Fig. 10(a).

TOF values of ca. 15–20 s^{-1} were previously reported for CH_4 reforming reactions (at 500 °C) for supported Rh and Ru catalysts with loadings ranging from 0.8–1.6 wt% for Rh (at 75% dispersion) and 1 wt% for Ru (at 30–50% dispersion) [14,18]. The dispersion of the 0.15 wt% Ru/γ-Al_2O_3 catalyst tested in our work was 27–39%, depending on measurement method (chemisorption or TEM). In another report, TOF values of 2.5–5 s^{-1} were reported for CH_4 dry reforming catalyzed by 1.6–3 wt% Ru/γ-Al_2O_3 (30–55% dispersion) at 600 °C [18], which is similar to the values we measured for the 3 wt% Ru catalyst (Fig. 10). For the commercial 12 wt% Ni/α-Al_2O_3 catalyst, we measured TOF ranging from 0.6–1.9 s^{-1} (depending on conditions and method of dispersion measurement), which is in the range of the values published in the literature [18].

Generally speaking, a monotonic, almost linear increase in TOF is expected for increasing active phase dispersion [14,18,20,21], which can be associated with decreasing metal loadings. However, the sudden drop observed for 0.07 wt% Ru is rather intriguing, though it can be apparently attributed to the lower dispersion of the 0.07 wt% Ru formulation (Fig. 9(e)). We hypothesize that the 0.07 wt% Ru catalyst featured a relatively large fraction of sub-nanometer Ru clusters (undetectable by TEM) that can form due to the exceptionally low Ru loading [22]. Since the tendency of nanoparticles to become oxidized increases with decreasing particle size [14], such clusters are expected to easily undergo oxidation under reforming conditions, resulting in reduced activity.

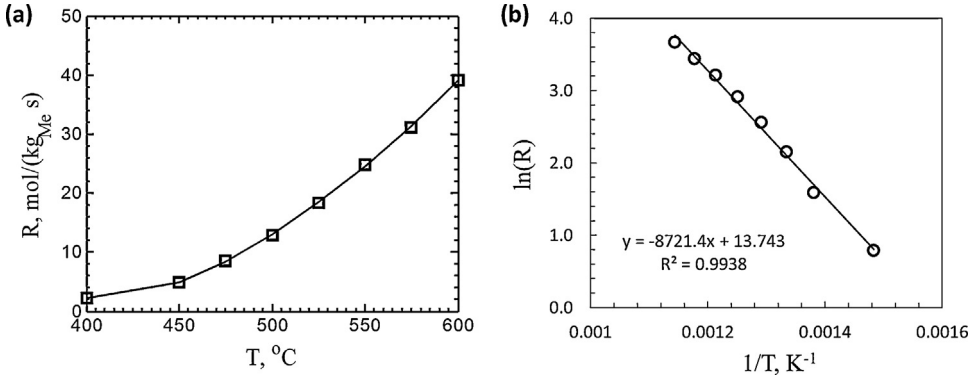

Fig. 11. Activation energy for 0.15 wt% Ru/γ-Al_2O_3 catalyst. Rate of CH_4 conversion (a) was measured at GHSV = 15,000 mL/(g h), P = 1 bar and S/C = 1 (CH_4 conversion was less than 15%). Activation energy of E = 72.5 kJ/mol was extracted (b).

The reduced activity of the 0.07 wt% Ru formulation could also result from the strong size-activity dependence, i.e. different intrinsic activity of surface sites with different coordination numbers, similar to that observed in Ru-catalyzed ammonia synthesis and decomposition [23–25]. The size of a metal nanoparticle affects the types of surface sites present and their relative abundance, which is particularly pronounced for small nanoparticles with sizes less than 10 nm. In a recent study, the catalytic performance of 0.1–5 wt% $Ru/\gamma\text{-}Al_2O_3$ catalysts (prepared by incipient wetness impregnation) in CO_2 reduction by H_2 (reverse WGS) was evaluated [22]. Notably, a strong dependence of both TOF and CO selectivity on the Ru loading was observed. The TOF decreased monotonically with decreasing Ru loadings for methanation reaction (CH_4 formation) and showed an optimum for reverse WGS at ca. 1–2 wt% Ru. This dependence was attributed to the different sizes of Ru nanoparticles obtained with different metal phase loadings. Interestingly, sub-nanometer Ru clusters were identified for the 0.1 wt% Ru formulation (by STEM).

Therefore, the optimum in TOF we observed for the 0.15 wt% Ru formulation (Fig. 10) could result from the optimum type and relative amount of surface sites obtained for Ru nanoparticles with the size of ca. 2 nm (Fig. 9(d)). However, our current data do not allow us to discriminate between the two options, of the oxidized sub-nanometer clusters for the 0.07 wt% Ru catalyst and of the strong size-activity relationship. Further studies are currently underway to understand the observed effects.

The apparent activation energy measured for the 0.15 wt% $Ru/\gamma\text{-}Al_2O_3$ catalyst was 72.5 kJ/mol (Fig. 11). This value is considerably lower than the apparent activation energy of 91 kJ/mol obtained by Wei and Iglesia in a kinetic study of CH_4 reforming over 3.2 wt% $Ru/\gamma\text{-}Al_2O_3$ catalysts (44.2% metal dispersion) prepared by incipient wetness impregnation [20]. However in another study with a 0.8–1.6 wt% Rh/ZrO_2 catalysts (47–69% metal dispersion), the authors reported an apparent activation energy of ca. 70 kJ/mol [14], which is similar to the value obtained in our study. A more detailed investigation is required to understand the reason for the lower activation energy obtained in our study as compared to the work by Wei and Iglesia for the 3.2 wt% $Ru/\gamma\text{-}Al_2O_3$ [20].

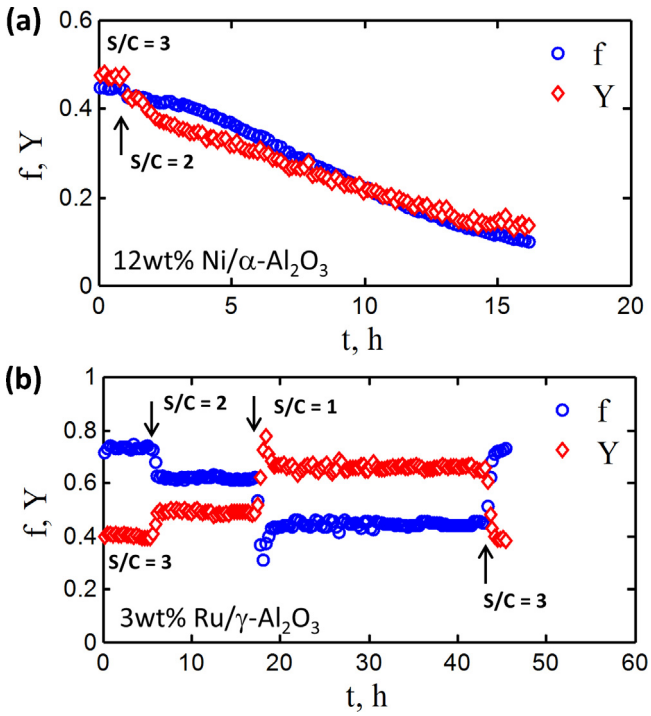

Fig. 12. Catalyst stability in low temperature methane steam reforming. Commercial 12 wt% $Ni/\alpha\text{-}Al_2O_3$ catalyst tested at $P = 1$ bar, $T = 600\,^{\circ}C$, $S/C = 2–3$, GHSV = 15,000 h^{-1} (a) and 3 wt% $Ru/\gamma\text{-}Al_2O_3$ catalyst tested at $P = 1$ bar, $T = 600\,^{\circ}C$, $S/C = 1–3$, GHSV = 4,500 h^{-1} (b) are compared in terms of CH_4 conversion (f) and CO selectivity (Y). Changes in applied steam-to-carbon ratio (S/C) are shown by arrows.

3.4. Stability

As we showed in the previous section, the ultra-low loading 0.15 wt% $Ru/\gamma\text{-}Al_2O_3$ catalyst is highly active, featuring TOF of ca. 40 s^{-1} at 600 °C. Herein, we discuss the issue of stability, which is frequently omitted in studies of catalysts for CH_4 reforming reactions.

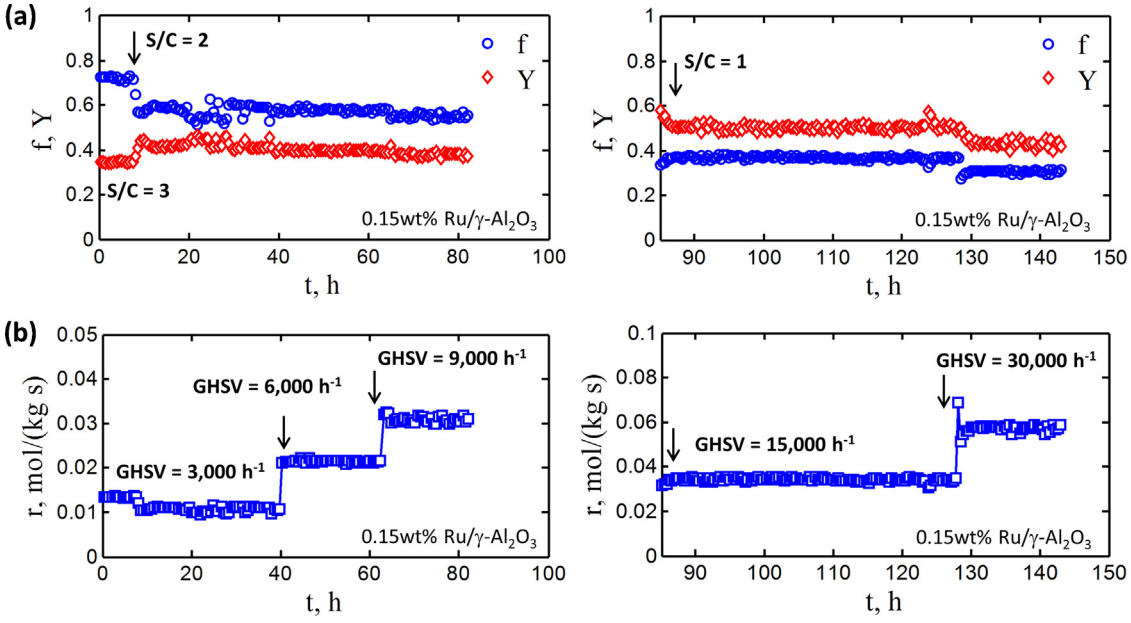

Fig. 13. Stability of the ultra-low loading $Ru/\gamma\text{-}Al_2O_3$ catalyst (0.15 wt% Ru) in low temperature methane steam reforming. Catalytic performance over the course of time (evaluated at $P = 1$ bar, $T = 600\,^{\circ}C$, $S/C = 1–3$ and GHSV = 3,000–30,000 h^{-1}) is shown in terms of CH_4 conversion and selectivity, f and Y (a), as well as in terms of corresponding rate of CH_4 conversion, r (b). Changes in S/C and GHSV throughout the course of the experiment are shown within the plots by arrows. Right panels represent the continuation of the data shown in left panels.

Fig. 12 compares the stability of the Ni-based (commercial) catalyst, as a reference, and of the 3 wt% Ru/γ-Al_2O_3 formulation which represents a typical Ru loading implemented in commercial Ru-based catalysts. The commercial Ni/α-Al_2O_3 catalyst was relatively stable at $S/C = 3$ but deactivated rapidly at $S/C = 2$, losing ca. 70% activity over the course of 15 h, Fig. 12(a). In contrast, the 3 wt% Ru/γ-Al_2O_3 catalyst was very stable not only at $S/C = 2$, but even at $S/C = 1$. The conversion and selectivity recovered to their initial values upon switching to $S/C = 3$ after almost 40 h on stream at low S/C values, Fig. 12(b). In fact, these observations were highly expected, since it is well-known that Ni-based catalysts easily deactivate at relatively low temperatures and steam-to-carbon ratios due to oxidation and coking, while PGM-based catalysts (e.g. Rh and Ru) are highly stable under these conditions [10].

Much more interestingly, the 0.15 wt% Ru/γ-Al_2O_3 formulation was also exceptionally stable in low temperature MSR, including low steam-to-carbon ratios and elevated space velocities. Fig. 13 shows the catalytic performance of the 0.15 wt% Ru catalyst over the time period of 145 h in terms of CH_4 conversion and CO selectivity, Fig. 13(a), as well as in terms of CH_4 conversion rate, Fig. 13(b). The stability was evaluated over the range of space velocities of GHSV = 3,000 – 30,000 h^{-1}. Starting from $S/C = 3$ and GHSV = 3,000 h^{-1}, the steam-to-carbon ratio was switched to $S/C = 2$ after 5 h and space velocity was stepwise increased to 9,000 h^{-1} (left panels in Fig. 13). For each space velocity tested over the 85 h period of time, no reduction in the rate of CH_4 conversion was observed. After 85 h, the steam-to-carbon ratio was switched to $S/C = 1$ and the throughput was further increased to GHSV = 15,000 h^{-1} and then to 30,000 h^{-1} (right panels of Fig. 13). No reduction in the CH_4 conversion rate was observed. Note that GHSV = 30,000 h^{-1} corresponds to a contact time of ca. 100 ms, which is in the range of contact times used in industrial steam reforming. The exceptional stability of the 0.15 wt% Ru/γ-Al_2O_3 catalyst is highly nontrivial. With such ultra-low loading and small nanoparticle size (ca. 2 nm, Fig. 9), the catalyst is highly susceptible to deactivation via oxidative routes, as it was reported for MSR catalyzed by 0.1 wt% Rh/ZnO_2 (50% reduction in intrinsic activity over 15 h) for example [14]. Our current data do not allow us to propose a mechanism for such exceptional stability and further investigation is underway.

4. Conclusions

Though catalysts based on platinum group metals feature high activity and stability in many heterogeneously-catalyzed reactions, including methane reforming, their price and availability limit their commercialization. Significantly reducing the active phase loading without sacrificing performance is crucial for industrial applications. Herein, we addressed this challenge by identifying the lower limit of the metal loading of the Ru/γ-Al_2O_3 catalyst that can provide high catalytic activity and, at the same time, excellent stability under reforming conditions. We show that the ultra-low loading Ru/γ-Al_2O_3 catalysts prepared by sonication-assisted wet impregnation exhibits excellent catalytic performance in low temperature methane steam reforming, targeting the application of solar thermal reforming via parabolic troughs.

The 0.15 wt% Ru/γ-Al_2O_3 formulation outperforms the commercial Ni-based catalyst (12 wt% Ni/α-Al_2O_3) by two orders of magnitude in terms of methane conversion rate per active metal loading and in turnover frequency. The catalyst also exhibits excellent stability at low steam-to-carbon ratios, which is of great importance for solar thermal reforming applications. The excellent performance of the 0.15 wt% Ru/γ-Al_2O_3 catalyst at industrially relevant space velocities makes it an attractive alternative to the existing commercial Ni-based catalysts, which are unsuitable for low temperature applications. The applicability to solar thermal reforming applications is yet to be tested since the use of concentrated solar power will impose additional requirements, such as stability with respect to a fluctuating heat source.

Our findings also show that there is a strong active phase loading-activity relationship, which is manifested as a pronounced optimum in the turnover frequency vs. Ru loading. We determined the lowest limit of the Ru loading as ca. 0.15 wt%. Below this limit, the catalyst activity declines significantly. A reason for this reduction in catalytic activity could be the formation of a large fraction of sub-nanometer Ru clusters, which can be easily oxidized, particularly under the low-temperature reforming conditions. Another reason could be significant differences in the intrinsic activity of various surface sites with different coordination numbers. These findings emphasize the importance of development of novel methods for catalyst nano-structuring. Ideally, such methods should allow us to maximize the number of the most active sites, while reducing the active phase loading as much as possible.

Acknowledgement

The authors highly appreciate and acknowledge the support of King Fahd University of Petroleum and Minerals (Dhahran, Saudi Arabia) through the research grant # R12-CE-10 offered by KFUPM-MIT Clean Water and Clean Energy Research Collaboration Center.

References

[1] M. Romero, A. Steinfeld, Energy Environ. Sci. 5 (2012) 9234–9245.
[2] A. Steinfeld, Solar Energy 78 (2005) 603–615.
[3] W.R. Wagar, C. Zamfirescu, I. Dincer, Int. J. Hydrogen Energy 36 (2011) 7002–7011.
[4] C. Agrafiotis, H. vonStorch, M. Roeb, C. Sattler, Renewable Sustainable Energy Rev. 29 (2014) 656–682.
[5] M.M. Wright, Y. Román-Leshkov, W.H. Green, Biofuels Bioprod. Biorefin. 6 (2012) 503–520.
[6] D.S.A. Simakov, M.M. Wright, S. Ahmed, E.M.A. Mokheimer, Y. Román-Leshkov, Catal. Sci. Technol. (2015), http://dx.doi.org/10.1039/c4cy01333f.
[7] J.-W. Snoeck, G.F. Froment, M. Fowles, J. Catal. 169 (1997) 250–262.
[8] J.-W. Snoeck, G.F. Froment, M. Fowles, J. Catal. 169 (1997) 250–262.
[9] M.C. Annesini, V. Piemonte, L. Turchetti, Chem. Eng. Trans. 11 (2007) 21–26.
[10] S.D. Angeli, G. Monteleone, A. Giaconia, A.A. Lemonidou, Int. J. Hydrogen Energy 39 (2014) 1979–1997.
[11] J. Wei, E. Iglesia, Phys. Chem. Chem. Phys. 6 (2004) 3754–3759.
[12] B.T. Schadel, M. Duisberg, O. Deutschmann, Catal. Today 142 (2009) 42–51.
[13] M.H. Halabi, M.H.J.M. deCroon, J. van-der-Schaaf, P.D. Cobden, J.C. Schouten, Appl. Catal. A Gen. 389 (2010) 68–79.
[14] D.A.J.M. Ligthart, R.A. vanSanten, E.J.M. Hensen, J. Catal. 280 (2011) 206–220.
[15] D. Qin, J. Lapszewicz, Catal. Today 21 (1994) 551–560.
[16] A. Berman, R.K. Karn, M. Epstein, Appl. Catal. A Gen. 282 (2005) 73–83.
[17] V.M. Shinde, G. Madras, Int. J. Hydrogen Energy 38 (2013) 13961–13973.
[18] G. Jones, J.G. Jakobsen, S.S. Shim, J. Kleis, M.P. Andersson, J. Rossmeisl, F. Abild-Pedersen, T. Bligaard, S. Helveg, B. Hinnemann, J.R. Rostrup-Nielsen, I. Chorkendorff, J. Sehested, J.K. Nørskov, J. Catal. 259 (2008) 147–160.
[19] D.S.A. Simakov, M. Sheintuch, AIChE J. 57 (2011) 525–541.
[20] J. Wei, E. Iglesia, J. Phys. Chem. B 108 (2004) 7253–7262.
[21] J. Wei, E. Iglesia, J. Phys. Chem. B 108 (2004) 4094–4103.
[22] J.H. Kwak, L. Kovarik, J.n. Szanyi, ACS Catal. 3 (2013) 2449–2455.
[23] J. Gavnholt, J. Schiøtz, Phys. Rev. B 77 (2008) 035404.
[24] A.M. Karim, V. Prasad, G. Mpourmpakis, W.W. Lonergan, A.I. Frenkel, J.G. Chen, D.G. Vlachos, J. Am. Chem. Soc. 131 (2009) 12230–12239.
[25] I. del Rosal, M. Mercy, I.C. Gerbe, R. Poteau, ACS Nano 7 (2013) 9823–9835.